NASA TECHNICAL NOTE

NASA TN D-4294

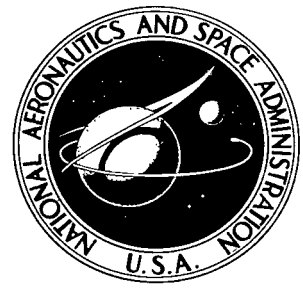

NASA TN D-4294

WAVEFORM DISTORTION IN A MAXIMUM-LIKELIHOOD DARLINGTON DETECTOR FOR M-ARY PFM SIGNALS

by Paul J. Heffernan

Goddard Space Flight Center
Greenbelt, Md.

NATIONAL AERONAUTICS AND SPACE ADMINISTRATION • WASHINGTON, D. C. • MARCH 1968

WAVEFORM DISTORTION IN A MAXIMUM-LIKELIHOOD DARLINGTON DETECTOR FOR M-ARY PFM SIGNALS

By Paul J. Heffernan

Goddard Space Flight Center
Greenbelt, Md.

NATIONAL AERONAUTICS AND SPACE ADMINISTRATION

For sale by the Clearinghouse for Federal Scientific and Technical Information
Springfield, Virginia 22151 – CFSTI price $3.00

ABSTRACT

This paper describes a proposed pulse-frequency modulation digital communication system for satellite applications. The heart of the proposed system is a maximum-likelihood detector of the spectrum-analysis type discussed by Darlington. It is shown that the proposed technique is in principle an ideal M-ary system. A general description is followed by an analysis of anticipated departures from the theoretic system—in particular, waveform distortion due to finite bandwidth, slope mismatch, and phase and amplitude ripple. General results are derived, from which permissible tolerances for departures from the theoretical system may be computed.

CONTENTS

WAVEFORM DISTORTION IN A MAXIMUM-LIKELIHOOD DARLINGTON DETECTOR FOR M-ARY PFM SIGNALS

by
Paul J. Heffernan
Goddard Space Flight Center

INTRODUCTION

This paper presents an analysis made at GSFC in 1966 to support a feasibility study for a time-division-multiplex system of multiple-access communications between pairs of small ground terminals via a subsynchronous earth-orbiting satellite.

The modulation-demodulation equipment has not been instrumented beyond breadboarding several critical elements; timing and synchronization hardware has been developed to engineering-model level and tested in satellite links.

While a brief discussion of communication system operation and anticipated performance is included for purposes of completeness, the main purpose of this paper is to predict the effects of amplitude and phase anomalies in a particular time-invariant linear system using classical Fourier integral techniques.

OVERALL SYSTEM OPERATION

General

This communication system furnishes duplex 4 kHz voice or data channels simultaneously to several pairs of users via an earth-orbiting satellite relay. All communication is in real time; multiple access is accomplished by time-division-multiplex (TDM). Multiple-access satellite communications have been treated extensively in the literature (References 1, 2, and 3), so it is enough to state here that of the three basic signal-multiplexing techniques available (time-division, frequency-division, and common-spectrum), TDM in theory provides the greatest channel capacity per user in situations where satellite transmitter power is the parameter limiting performance (References 4 and 5).

The modulation technique selected is 127-level quantized pulse-frequency modulation (PFM). Signal detection is by "spectrum analysis" pulse-frequency modulation to pulse-position modulation (PFM-PPM) conversion. This scheme was first discussed by Darlington in connection with threshold

extension for wideband FM signals (Reference 6). The 127-PFM signaling waveforms are pairwise orthogonal, and the Darlington demodulation process is essentially non-coherent matched-filter maximum-likelihood detection. Hence, the signaling scheme is in principle an ideal M-ary system (Reference 7). That is to say, the operations by which the receiver guesses which of the M signals was sent afford the least probability of error possible with non-coherent reception (in the absence of subsequent error detection and/or correction).

Timing and Synchronization

This discussion of timing and synchronization is included in order to define the communication system under consideration and is not a description in depth. The interested reader is referred to Reference 8 for a complete description of system timing and synchronization subsystems and to Reference 9 for the results of timing and synchronization subsystem performance in closed-loop satellite tests.

Up to ten ground stations may participate in the system; only one station at a time uses the satellite. Hence, the system provides a maximum of ten simplex links or (when pairs of ground stations communicate with each other) up to five duplex links.

The system centers around a timing frame that contains one master synchronization burst and ten information bursts, one for each simplex link. There are 8000 frames per second, so that no storage or buffering is required for transmission of voice or data signals bandlimited to 4 kHz (assuming periodic Nyquist sampling) as long as only one such 4 kHz signal is to be transmitted per simplex link. (See Figure 1.)

Of the participating ground stations, one is called the master station; the rest are called slave stations. The master station controls all system timing. In each frame, the master station transmits the master synchronization burst from which all slave stations derive their timing. This burst is pre-programmed to be an rf pulse modulated in frequency at 800.00 kHz and repeated at intervals of 125.00 microseconds where these values hold at the satellite. Because the satellite is in motion with respect to master and slave stations, Doppler effects must be considered in signal pre-programming.

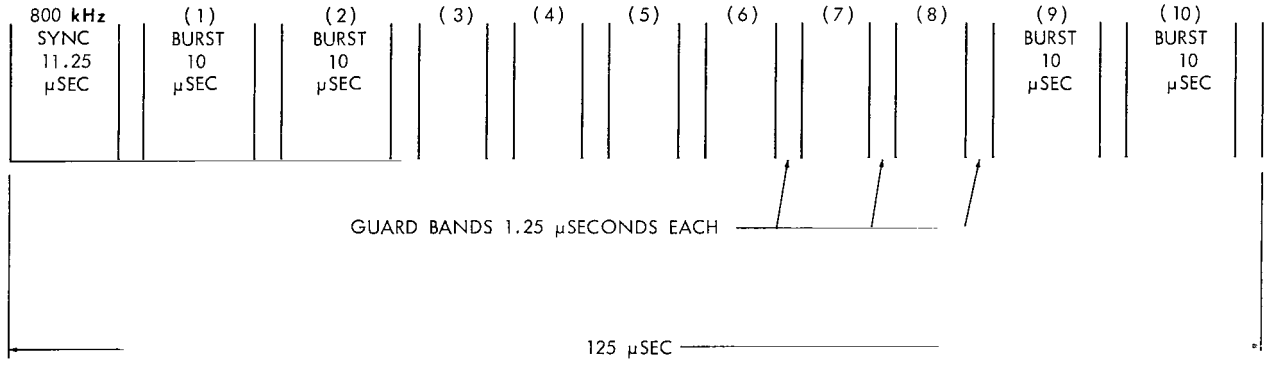

Figure 1—Format diagram.

Each slave station monitors the master synchronization burst upon its transmission back from the satellite to derive slave local timing. Because of the Doppler effect, local timing will differ somewhat (in any case less than a small fraction of 1 percent) from the exact 125.00 microsecond frame rate at the satellite; in general, local timing will differ slightly for each ground station in the system.

Once local framing is derived, intraframe timing must be established to prevent ground-station transmissions from overlapping upon arrival at the satellite. Intraframe timing is required also for operation of the signal demodulation equipment at each ground station—see below.

As already noted, techniques and hardware for establishing and maintaining these timing and synchronization functions have been developed, proven, and documented; further details of TDM system timing and synchronization are not given here. The proper subject of discussion is a point-to-point communication system in which 4 kHz signals are transmitted as sampled data; sampling intervals and instants being known with arbitrary precision and accuracy at both ends of the link, while rf carrier phase is unknown.

Pulse-frequency Modulation and Darlington Detection

PFM has been used with considerable success in numerous telemetry applications (Reference 10), but few attempts have been made to use this efficient M-ary signaling technique in communications systems for voice and data transmission.

The information signal to be transmitted is assumed to be an analog waveform bandlimited to 4 kHz and sampled periodically at the Nyquist rate; the clamped samples drive a quantized voltage-controlled oscillator to produce a train of rather low duty-cycle FM pulses as shown in Figure 2.

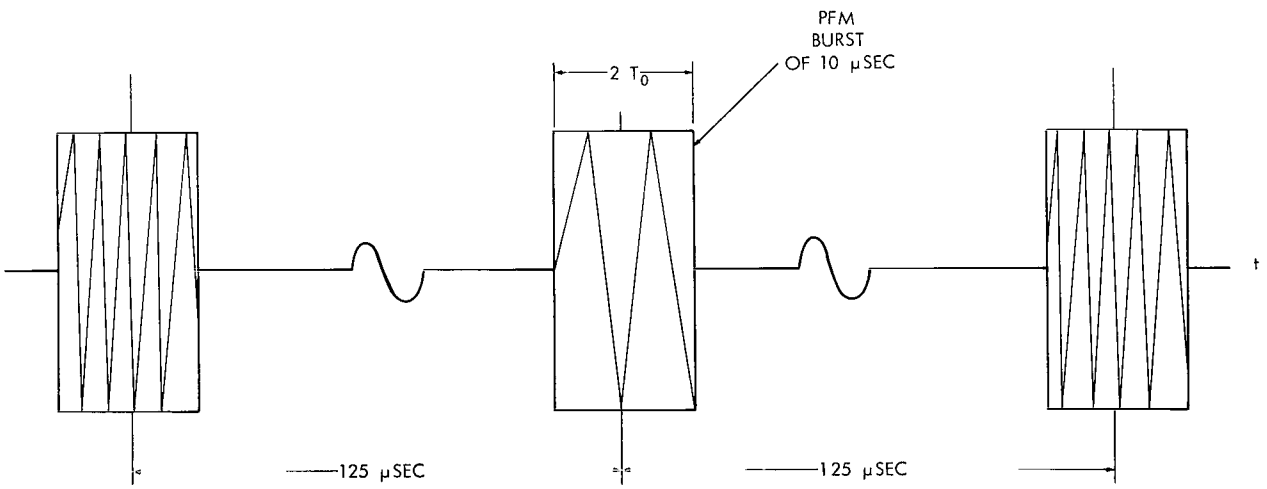

Figure 2—PFM signals.

A single pulse is of the form

$$S_N(t) = \cos 2\pi (f_c + \delta f)\, t \,, \qquad -T_0 \le t \le T_0 \tag{1}$$

where

f_c = reference carrier frequency

δf = 100 kHz (basic increment of discrete frequency modulation)

$N = 0, \pm 1, \pm 2, \cdots, \pm 64$

$T_0 = 5\ \mu$sec

The interval between pulses is

$$T_s = 125\ \mu\text{sec}$$

and corresponds to the Nyquist rate for 4 kHz signals. The discrete frequency modulation $N\delta f$—constant during any one pulse but changing from pulse to pulse in accordance with the amplitude samples of the information signal—is selected to be an integral multiple of the reciprocal of pulse width $2T_0$. As a consequence and despite their overlapping spectra, the 127 signaling waveforms are pairwise orthogonal over the signaling interval (Reference 11).

The amplitude resolution of the system is identical with that of seven-bit pulse-code modulation and, as with PCM, logarithmic or piecewise linear encoding would normally be used to reduce the effects of quantization distortion (Reference 12).

The optimum non-coherent detector for these PFM waveforms may be visualized as a bank of 127 matched filters whose outputs are envelope-detected and sampled at the anticipated instant of match to select the filter with the greatest response (Reference 13). The filter matched to the Nth signaling waveform $S_N(t)$ would have a system function $H_N(f)$ given by the complex conjugate of the spectrum of $S_N(t)$:

$$H_N^*(f) = \int_{-\infty}^{\infty} S_N(t)\, e^{-i2\pi ft}\, dt \,. \tag{2}$$

Equivalently, the impulse response $h_N(t)$ of the Nth matched filter would be the $S_N(t)$ waveform run backward in time:

$$h_N(t) = S_N(-t) = S_N(t) \,. \tag{3}$$

Figure 3 is a block diagram of this PFM demodulator. Such systems have been instrumented for small alphabets (Reference 14); but for large alphabets (e.g., $M = 127$) the hardware would be unwieldy and expensive.

The alternate detection scheme shown in Figure 4 is a slight variant of a technique proposed by Darlington and referenced above. The 127 matched filters are replaced by a single circuit consisting of a function generator, a mixer, a dispersive delay line, and a tapped non-dispersive delay line. The operation of the detector may be described as follows.

The signal to be detected is $S_N(t)$ as given by Equation 1. It is mixed with $f(t)$, the output of the function generator. This function generator waveform is a linear FM pulse described by

$$f(t) = \cos 2\pi \left(f_r t + \frac{\mu t^2}{2} \right) , \qquad -T_0 \le t \le T_0 \tag{4}$$

where f_r is an unspecified reference frequency. The instantaneous frequency $f(t)$ is given by the time derivative of the phase and is

$$f_i(t) = f_r + \mu t , \qquad -T_0 \le t \le T_0 \tag{5}$$

where $\mu = 1.28 \times 10^{12}$ Hz/second.

The instantaneous frequency is thus a linear function of time (see Figure 5). After mixing and removal of out-of-band spurious responses, the signal driving the dispersive delay line is of the form

$$x_N(t) = \cos 2\pi \left[(f_0 + N\delta f)t + \frac{\mu t^2}{2} \right] , \qquad -T_0 \le t \le T_0 \tag{6}$$

where $f_0 = f_c + f_r$ is the carrier frequency of the pulse, and both the discrete frequency modulation $N\delta f$ and the linear frequency modulation $\mu t^2/2$ are present.

The response of the dispersive delay line to the excitation $x_N(t)$ can be determined using the Fourier integral. The complex system function of the delay line is modeled (for present purposes) as

$$H(f) = A(f)\, e^{i\phi(f)} , \tag{7}$$

where the amplitude characteristic $A(f)$ is that of an all-pass structure,

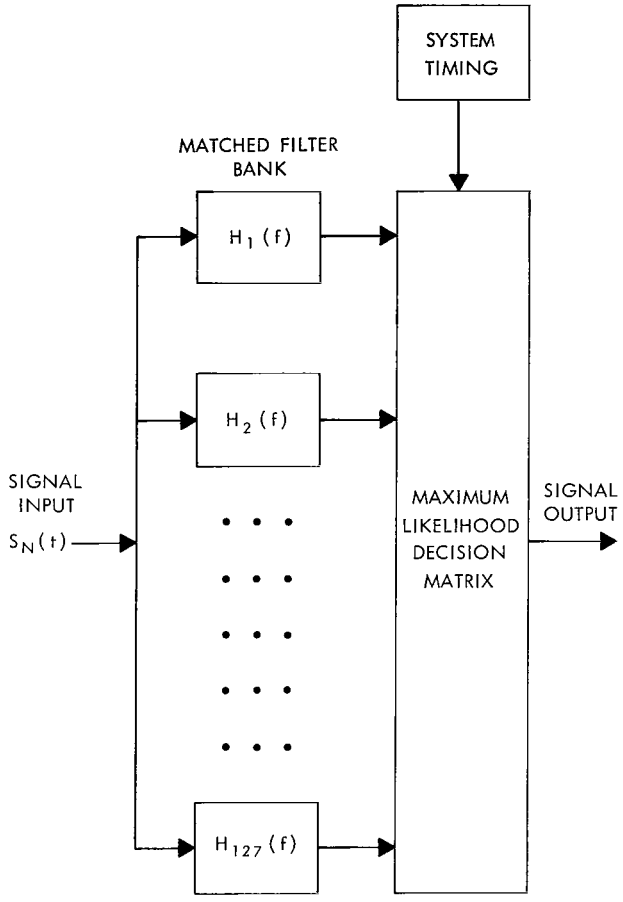

Figure 3—Filter bank PFM detector.

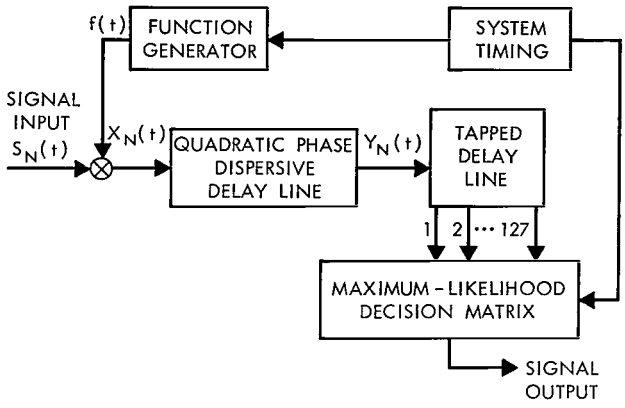

Figure 4—Darlington PFM detector.

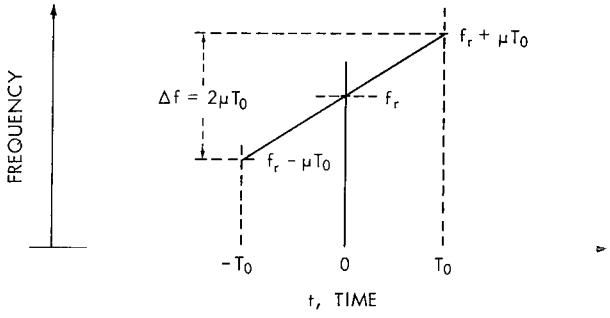

Figure 5—Instantaneous frequency of f(t) vs time.

$$A(f) = 1 , \qquad -\infty \leq f \leq \infty \tag{8}$$

and the phase characteristic is

$$\phi(f) = \frac{\pi}{\mu}\left(f - f_0\right)^2 - 2\pi f t_0 . \qquad -\infty \leq f \leq \infty \tag{9}$$

The time delay vs frequency for this structure is

$$\tau(f) = t_0 + \frac{f_0 - f}{\mu} \tag{10}$$

Parameter t_0 represents an arbitrary constant delay; the $f_0 - f/\mu$ term represents a delay that decreases linearly with increasing (positive) frequency. (See Figure 6.) Structures or filters of this type are usually termed dispersive, because they delay the spectral components of an arbitrary excitation non-uniformly and hence tend to spread out or disperse the signal in time.

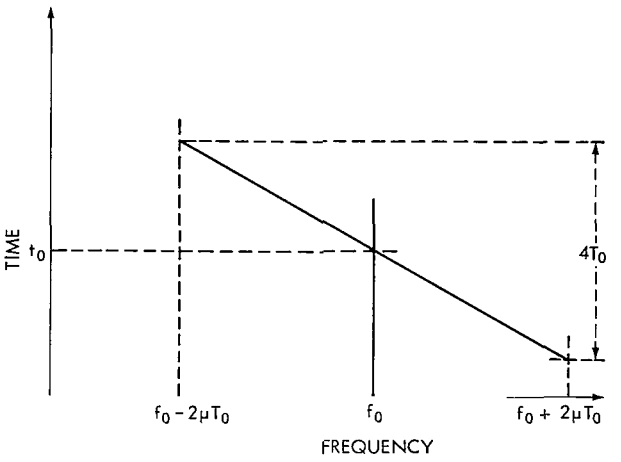

Figure 6—Time delay vs frequency of dispersive delay line.

This need not always be true. For instance, if the input is as given in Equation 6, the unit amplitude rectangular-envelope input pulse is compressed into a narrow, peaked $(\sin x)/x$ pulse, where the time to peak is determined by the discrete frequency-modulation $N\delta f$ and the overall network delay t_0. This is evident from an expression for network response. Let

$$y_N(t) = \left|\tilde{y}_N(t)\right| = \left|x(t) * h(t)\right| , \tag{11}$$

where

$$h(t) = \int_{-\infty}^{\infty} A(f)\, e^{i\phi(f)}\, e^{i2\pi ft}\, df . \tag{12}$$

Taking $A(f)$ equal to unity, corresponding to the postulated all-pass amplitude characteristic, and with $\phi(f)$ given by Equation 9, the response is a rather complicated FM waveform whose envelope is given by

$$y_N(t) = \sqrt{4\mu T_0^2}\left|\frac{\sin 2\pi T_0\left[\mu\left(t - t_0\right) + N\delta f\right]}{2\pi T_0\left[\mu\left(t - t_0\right) + N\delta f\right]}\right| . \tag{13}$$

This result is derived in Appendix A. Before studying the properties of this response, we simplify Equation 13 as follows: The overall filter delay t_0 is significant because it determines how far structures may be approximated at the frequency of interest. But—for purposes of signal analysis—it is an arbitrary parameter that can be set equal to zero. The response is then

$$y_N(t) = \sqrt{4\mu T_0^2}\left|\frac{\sin 2\pi T_0\left[\mu t + N\delta f\right]}{2\pi T_0\left[\mu t + N\delta f\right]}\right| . \tag{14}$$

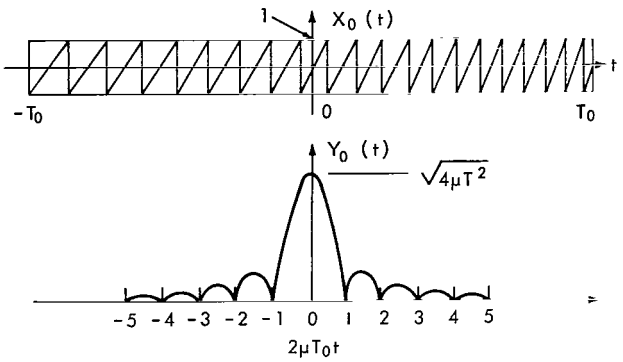

Figure 7—Input and output waveforms for the Darlington PFM detector.

Input and simplified output waveforms are shown in Figure 7 for the case N = 0. Equations 6 and 14 and Figure 7 indicate that an effective pulse compression has taken place and that the discrete PFM has been converted to a discrete PPM.

Associated with and characterizing the pulse compression phenomenon is a signal processing gain Γ which may be defined as the ratio of output to input pulse peak power:

$$\Gamma = 4\mu T_0^2 . \tag{15}$$

In the present system where

$$\mu = 1.28 \times 10^{12} \text{ Hz}$$

and

$$T_0 = 5 \ \mu\text{sec} ,$$

we have

$$\Gamma = 128 , \quad \text{i.e.,} \quad 21.0 \text{ db} . \tag{16}$$

This signal-processing gain* is a fundamental figure of merit for the general pulse-compression phenomenon because Γ, as defined above, is a measure of the pulse-width compression ratio. With reference to Figure 7, output-pulse width is defined in terms of its (approximate) half-power points; the ratio of input to output pulse widths is

$$2T_0 \div \frac{1}{2\mu T_0} = 4\mu T_0^2 = \Gamma .$$

Γ may also be considered a time-bandwidth product, that is, the product of the duration and total frequency sweep of the input rectangular-envelope frequency-modulated pulse:

$$(2T_0)(2\mu T_0) = 4\mu T_0^2 = \Gamma .$$

*Also termed dispersion factor in the literature of pulse-compression radar.

The PFM-to-PPM conversion process is the heart of the Darlington demodulator. For $N \neq 0$ the $y_N(t)$ waveform peaks at

$$t = \frac{N\delta f}{\mu} \qquad N = \pm 1, \pm 2, \cdots, \pm 64 \tag{17}$$

and for any N, the nulls of $y_N(t)$ occur at

$$t = \frac{N\delta f}{\mu} \pm \frac{M}{2\mu T_0} \cdot \qquad M = \pm 1, \pm 2, \cdots \tag{18}$$

The system parameters have been selected so that

$$\delta f = \frac{1}{2T_0} \cdot$$

Therefore, the output waveforms $y_N(t)$ interlace peaks and nulls as shown in Figure 8. This quasi-orthogonality of the $y_N(t)$ is, of course, due to the orthogonality of the original signaling waveforms and is the basis for the subsequent maximum-likelihood detection.

The output of the dispersive delay line drives a non-dispersive tapped delay line. Taps are located at intervals of $(2\mu T_0)^{-1}$ or about 78 nanoseconds corresponding to the pulse intervals indicated in Figure 8. Using techniques of the general type outlined in Reference 14, the tap with the greatest response is selected to complete signal detection.

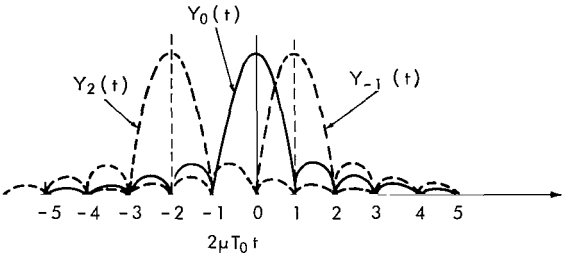

Figure 8—Quasi-orthogonality of the output waveforms.

Signal-to-noise Ratios and Error Rates

It is stated above that the PFM communication technique using Darlington detection described here is essentially an ideal M-ary system of the type discussed by Turin. The theoretical performance of such systems has been studied for some time and is well documented. References 7, 10, 14, 15, 16, and 17 are especially relevant.

This paper is designed not to reproduce or summarize such results but to show that the present scheme is indeed an ideal M-ary system. To do this it is enough to show that the signal-to-noise ratio* at the output of the dispersive delay line in Figure 4 is just what would be obtained at the output of the matched filter containing the signal in Figure 3.

*In the usual sense of peak signal to mean-square noise power ratio under conditions of signal reception in wide-sense stationary white gaussian noise.

If the received signal is immersed in noise of (two-sided) spectral density $\eta/2$, the signal-to-noise ratio at the output of the Nth matched filter of Figure 3 at the instant of match is the "energy contrast ratio," i.e., the ratio of signal energy to noise spectral density:

$$\frac{2}{\eta}\int_{-\infty}^{\infty} S_N^2(t)\,dt = \frac{2T_0}{\eta} . \tag{19}$$

To compute the signal-to-noise ratio that can be obtained with the present system, we must identify the equivalent noise bandwidth of the overall demodulator. The derivation of Equation 13 in Appendix A assumes an all-pass amplitude characteristic for the dispersive delay line and associated transmission system, and leads to an output signal-to-noise ratio of zero; i.e., an infinite system-noise bandwidth. Actually it can be asserted that system bandwidths are finite, if only to ensure the realization of the dispersive delay line (or a suitable approximating structure) at the frequencies of interest. What is the noise bandwidth of the system?

It is shown in Appendix B that the appropriate noise bandwidth of the dispersive delay line proper is twice the total frequency sweep $2\mu T_0$ of any one of the $x_N(t)$. Provided that all prior structures are broadband, the system noise bandwidth is $4\mu T_0$, i.e., 25.6 MHz. For this case, we can compute the signal-to-noise ratio as follows.

From Equation 13, the peak signal power is

$$\left[y_N^2(t)\right]_{max} = 4\mu T_0^2$$

and from the above discussion the mean-square noise power is

$$4\eta\mu T_0 .$$

This leads to a signal-to-noise ratio of

$$\frac{4\mu T_0^2}{4\eta\mu T_0} = \frac{T_0}{\mu} , \tag{20}$$

which is 3 db poorer than that attained in the matched filter case.* If we could narrow the system noise bandwidth to $2\mu T_0$ (as in chirp-radar systems for detection of a single known signal) the dispersive delay-line detector would have the same signal-to-noise ratio as the matched filter, as argued in Reference 19.

*Actually, the situation is somewhat more involved than the above argument indicates. The function generator waveform f(t) effectively gates the input noise process on and off and creates a non-stationary noise process at the output of the Darlington detector. Applying the analysis given in Reference 18 to the present system shows that the variance of the non-stationary output noise process has the constant value $4\mu n T_0$ (for the present case where we assume no signal prefiltering) throughout the signal observation interval.

In fact, we can narrow the system noise bandwidth to a value closely approaching $2\mu T_0$ (although the dispersive delay line needs $4\mu T_0$ for effective PFM-to-PPM conversion of rectangular-envelope chirp signals)—prefilter the input signals $S_N(t)$ by suppressing all energy outside the band (considering now positive frequencies only) $f_c \pm 6.4$ MHz. This operation eliminates all out-of-band sidelobes of the $\sin x/x$ spectra of the $S_N(t)$ but need not affect in-band spectra in any way. As a consequence, there will be a new set of signals $S_N'(t)$ which within the band have the same spectra as the original $S_N(t)$ but outside the band have different (i.e., highly attenuated) spectra. After mixing with $f(t)$, the waveforms into the dispersive delay line will be of the form (using complex notation)

$$\tilde{x}_N'(t) = \epsilon_N'(t)\, e^{i2\pi\left[(f_0+N\delta f)t+\mu t^2/2\right]}, \qquad -T_0 \le t \le T_0 \tag{21}$$

where $\epsilon_N'(t)$ is a non-rectangular envelope function corresponding to the inverse Fourier transform of the spectrum of $S_N'(t)$. If we ignore the explicit form of $\tilde{x}_N'(t)$, the quadratic phase dispersive delay line produces an output signal $\tilde{y}_N'(t)$ whose envelope is the Fourier transform of $\epsilon_N'(t)$ (see Appendix A). Within the signal observation interval, the $\tilde{y}_N'(t)$ appears as pure $\sin x/x$ waveforms whose peaks and nulls interlace as discussed above; outside the observation interval, the response of the delay line is highly attenuated.

This effect may be visualized by picturing the time response of the dispersive delay line as a scaled replica of the spectra of the prefiltered input waveforms; if prefiltering does not alter the spectra within the band $f_c \pm 6.4$ MHz, the time response of the dispersive delay line will not be altered or distorted within the observation interval; signal detection will be affected only in improving the signal-to-noise ratio of Equation 20 by an amount approaching 3 db. Hence, the present system, in the limit for perfect signal prefiltering and with a perfect Fourier-transforming dispersive delay line, yields the same signal-to-noise ratio as a bank of perfect correlators or matched filters.

WAVEFORM DISTORTION IN THE DARLINGTON DEMODULATOR

Souces of Waveform Distortion and Philosophy of Analysis

The derivation of the dispersive delay line response to the excitation $x_N(t)$ as given in Appendix A assumes an infinite bandwidth system with unity all-pass amplitude characteristic and pure quadratic phase characteristic for all frequencies. A practicable system can, of course, only approximate these characteristics in some finite band, and it is to be expected that the actual output waveforms obtained will differ somewhat from those shown in Figures 7 and 8.

Such departures from pure $(\sin x)/x$ waveforms are termed distortion and will, in general, produce two effects that may be considered separately. First, there will probably be some loss in

signal-processing gain Γ relative to the theoretical value of 128 or 21 db and second, the delicate quasi-orthogonality of the output waveforms will probably be destroyed to some extent, as the peaks and nulls may not interlace perfectly according to the scheme shown in Figure 8.

This paper does not consider how far these distortions can be tolerated. It seeks general formulations characterizing losses in Γ and destruction of sidelobe interlacing in terms of departures from ideal signals and networks considered in Appendix A. Emphasis is placed not on actual details of output signal waveshapes, but on loss in peak response (reflected in smaller output signal-to-noise ratios) and the rise, if any, of the $(\sin x)/x$ sidelobe level at the expected nulls, particularly those adjacent to the main response (see Figure 8).

Potential sources of waveform distortion are finite system bandwidth, slope mismatch (Figures 5 and 6) of the dispersive delay line relative to the sweep rate of the function generator, phase ripples or fluctuations within the system passband, and amplitude ripples within the system passband. Each of these departures from the ideal is considered below in terms of classical linear system theory.

Effects of Finite Bandwidth

The formal derivation of Equation 13 given in Appendix A ignores the fact that the dispersive delay line itself, as well as the rest of the transmission system, is a bandpass rather than an all-pass structure. The response in the finite bandwidth case can be found using the Fourier integral. With reference to Appendix B, the signal $x_N(t)$ has a spectrum $X_N(f)$ given by

$$X_N(f) = \frac{e^{-i(\pi\alpha^2/\mu)}}{2\sqrt{2\mu}}\left[Z(\xi_1) - Z(\xi_2)\right], \qquad f > 0 \tag{22}$$

where

$$\alpha = f_0 - f + N\delta f$$

and

$$\xi_{\substack{1\\2}} = \sqrt{\frac{\Gamma}{2}}\left(\frac{2\alpha}{\Delta f} \pm 1\right).$$

The general expression for the finite bandwidth response is then given by

$$y_N(t) = \left|\int_{-\infty}^{\infty} X_N(f) H_f(f) e^{i2\pi ft}\, df\right|, \tag{23}$$

where the magnitude of $H_f(f)$ is zero except where

$$f_0 - 2\mu T_0 \leq f \leq f_0 + 2\mu T_0 \qquad f > 0$$

and

$$H_f(-f) = H^*(f)$$

$$X_N(-f) = X_N^*(f) .$$

Then

$$y_N(t) = \frac{1}{\sqrt{2\mu}} \left| \int_{f_0-\Delta f}^{f_0+\Delta f} e^{i(\pi/\mu)(f_0-f)^2} e^{-i(\pi/\mu)\alpha^2} \left[Z(\xi_1) - Z(\xi_2) \right] e^{i2\pi ft} \, df \right| . \tag{24}$$

This integral has been evaluated in general terms by DiFranco (Reference 20) and his result (for a chirp radar system with $\Gamma = 50$) shown, together with the theoretical $|(\sin x)/x|$ curve, in Figure 9. Unfortunately, his integrated expression is so complex and lengthy that little is to be gained by reproducing it here. Nevertheless, in view of the signal-processing loss and sidelobe distortion evident in Figure 9, formulas should be obtained for the peak response and the response at the adjacent nulls in accordance with the analytic philosophy outlined above.

To determine the peak response, we rewrite Equation 24:

$$y_N(t) = \frac{1}{\sqrt{2\mu}} \left| \int_{f_0-\Delta f}^{f_0+\Delta f} \left[Z(\xi_1) - Z(\xi_2) \right] e^{i(2\pi/\mu)(\mu t + N\delta f)} \, df \right| . \tag{25}$$

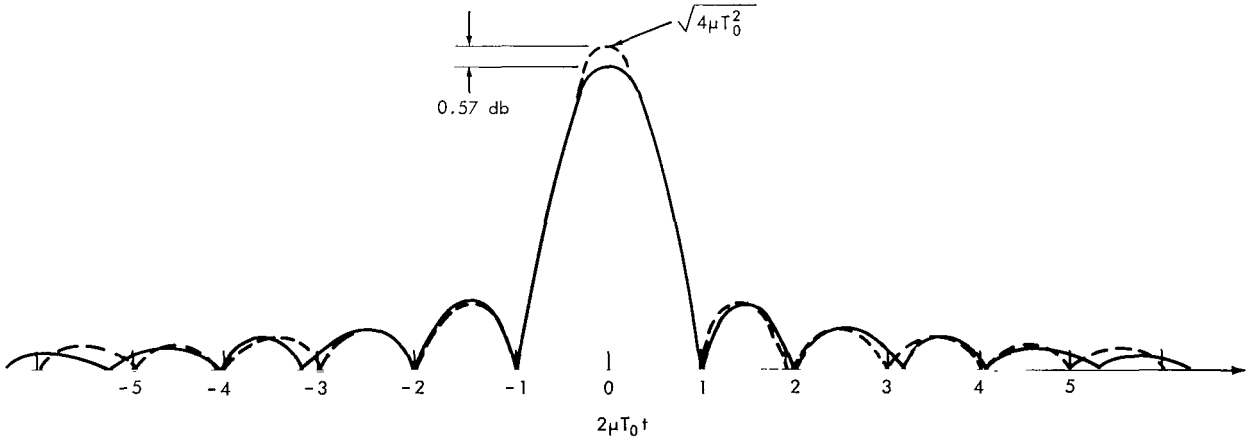

Figure 9—DiFranco's finite bandwidth output waveform, T = 50.

The peak response is anticipated at $t = -N\delta f/\mu$:

$$y_N\left(-\frac{N\delta f}{\mu}\right) = \frac{1}{\sqrt{2\mu}}\left|\int_{f_0-\Delta f}^{f_0+\Delta f}\left[Z(\xi_1) - Z(\xi_2)\right] df\right| . \tag{26}$$

Introducing a normalized discrete frequency modulation, $\delta_N = 2N\delta f/\Delta f$, and integrating with respect to $\theta = \alpha/\Delta f$, yields

$$y_N\left(-\frac{N\delta f}{\mu}\right) = \frac{\Delta f}{\sqrt{2\mu}}\left|\int_{-1+(\delta N/2)}^{1+(\delta N/2)}\left\{Z\left[\sqrt{\frac{\Gamma}{2}}(2\theta+1)\right] - Z\left[\sqrt{\frac{\Gamma}{2}}(2\theta-1)\right]\right\}d\theta\right| . \tag{27}$$

Using the formula for the definite integral of $Z(x)$ which is given in Appendix C, we write Equation 27 as

$$y_N\left(-\frac{N\delta f}{\mu}\right) = \sqrt{\frac{\Gamma}{8}}\left|(\delta_N+3)Z\left[\sqrt{\frac{\Gamma}{2}}(\delta_N+3)\right] + (\delta_N-3)Z\left[\sqrt{\frac{\Gamma}{2}}(\delta_N-3)\right] - (\delta_N+1)Z\left[\sqrt{\frac{\Gamma}{2}}(\delta_N+1)\right] - (\delta_N-1)Z\left[\sqrt{\frac{\Gamma}{2}}(\delta_N-1)\right]\right| . \tag{28}$$

This result reduces to the infinite-bandwidth case if Γ is large enough so that the several Fresnel integrals can be replaced by their values at infinity, i.e.

$$Z(\pm\infty) = \pm\left(\frac{i+1}{2}\right),$$

whence

$$y_N^2\left(-\frac{N\delta f}{\mu}\right) = \frac{\Gamma}{8}|2+2i|^2 = \Gamma .$$

Cases of interest are $\delta_N = 0, \pm 1$, corresponding to pulse spectra at the center and extreme edges of the system pass band. Operation on Equation 28, using asymptotic forms for Fresnel integrals of argument greater than 20 (Appendix C), shows that peak response is only down by some 0.1 db in the cases $\delta_N = 0, \pm 1$. The situation will be similar for intermediate values of δ_N, and, in view of other anticipated system losses, finite bandwidth is not a serious consideration—at least as regards losses in processing gain. It remains to be seen how much sidelobe distortion (as is evident in DiFranco's $\Gamma = 50$ case) will be present in the output waveforms.

The Nth null of the Nth output pulse occurs at $t = -5f/\mu(N+M)$, and we proceed, as above, to evaluate Equation 25 for this particular value of time. Again we use the normalized discrete frequency modulation δ_N, as defined above, but this time the integration is with respect to the arguments of the Fresnel integrals. After undergoing several elementary manipulations, the expression

for the output signal amplitude at the Mth anticipated null of the Nth output waveform is

$$y_N\left[-\frac{\delta f}{\mu}(N+M)\right] = \sqrt{\mu T_0}\left|\int_{\sqrt{\Gamma/2}(\delta_N-1)}^{\sqrt{\Gamma/2}(\delta_N+3)} Z(\xi_1)\, e^{-i2\pi(N+M)\sqrt{2/\Gamma}\xi_1}\, d\xi_1 - \int_{\sqrt{\Gamma/2}(\delta_N-3)}^{\sqrt{\Gamma/2}(\delta_N-1)} Z(\xi_2)\, e^{-i2\pi(N+M)\sqrt{2/\Gamma}\xi_2}\, d\xi_2\right| \quad (29)$$

These integrals may be recognized as truncated Fourier transforms of the Fresnel integral from ξ_1, ξ_2 space respectively into the discrete $(N+M)\sqrt{2/\Gamma}$ space. For any combination of the indices N and M, Equation 29 can be written out directly in terms of Fresnel integrals using the general formula for

$$\int_{x_1}^{x_2} Z(x)\, e^{-i2\pi yx}\, dx ,$$

given in Appendix C. Because of its length, the integrated expression will not be given explicitly here. For the system in question, several computations were made (in particular, for $N = 0$ and $M = 1, 3$; the sidelobe level at these points was more then 50 db below the main response.

For large Γ, the limits of the integrals diverge and the integrals tend to cancel. This agrees with the result that signal-processing gain is the same for both finite and infinite bandwidth situations for large Γ, and reflects the fact that for large Γ the linear FM pulse tends to have a rectangular frequency spectrum (Appendix B).

Effects of Slope Mismatch

With reference to Figures 5 and 6, the dispersive delay line should have a linear group-delay characteristic whose slope is the reciprocal of the frequency-vs-time slope of the function generator waveform $f(t)$. Departure from exact matching of the overall slopes produces waveform distortion in the $y_N(t)$. Slope mismatch ("quadratic phase distortion") is discussed in some detail in the literature of chirp radar, but it seems that there are no explicit equations for losses in Γ and the behavior of anticipated nulls. The desired equations are derived here by an approximation evolving in Reference 19.

Figure 10 illustrates the desired quadratic phase characteristic of the dispersive delay line, and also a phase characteristic corresponding to slope mismatch. With reference to Equation 11 (here renumbered),

$$\tilde{y}_N(t) = x_N(t) * h(t) , \quad (30)$$

the response in the presence of quadratic phase distortion of the type shown in Figure 10 is given by the magnitude of the convolution of $\tilde{y}_N(t)$ with the impulse response of a fictitious linear filter

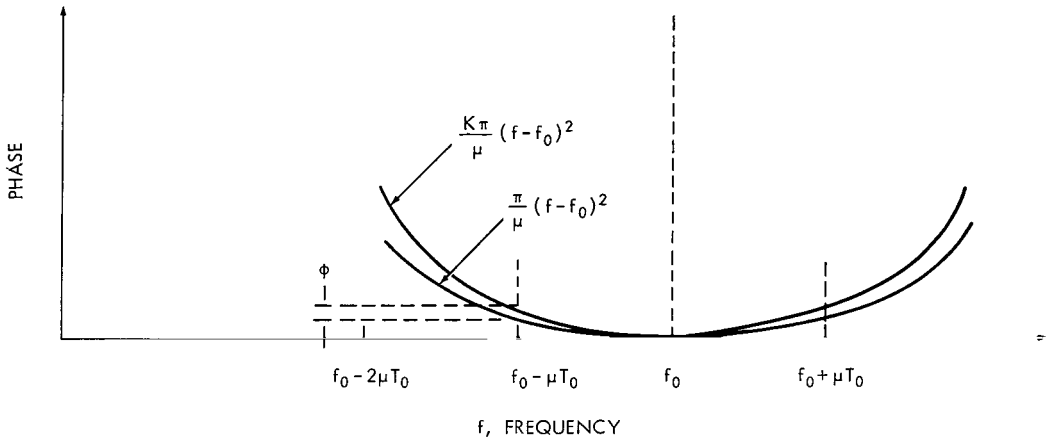

Figure 10—Quadratic phase distortion.

of system function

$$H_\phi(f) = e^{i(k-1)\pi/\mu(f-f_0)^2} . \tag{31}$$

For slope mismatch the same across the band, the *waveshapes* of all output signals are the same for all N. In the case of N = 0,

$$y_\phi(t) = \left| \int_{-\infty}^{\infty} \int_{-\infty}^{\infty} \tilde{y}_0(\tau)\, e^{i\left[(k-1)\pi/\mu(f-f_0)^2\right]}\, e^{i2\pi f(t-\tau)}\, df\, d\tau \right| . \tag{32}$$

The quadratic phase distortion is conveniently characterized by a phase shift ϕ measured at $f_0 \pm \mu T_0$, as shown in Figure 10:

$$\phi = \left| (k-1)\pi\mu T_0^2 \right| , \tag{33}$$

and, with this convention, Equation 32 becomes

$$y_\phi(t) = \left| \int_{-\infty}^{\infty} \int_{-\infty}^{\infty} \tilde{y}_0(\tau)\, e^{i\phi(f-f_0)/\mu T_0}\, e^{i2\pi f(t-\tau)}\, df\, d\tau \right| . \tag{34}$$

It does not appear possible to evaluate this integral exactly. An approximation discussed in Reference 19 ignores a residual frequency in $\tilde{y}_0(t)$. This is permissible because the effective duration of $\tilde{y}_0(t)$ is short. This approximation is equivalent to assuming that the envelope of $x_N(t)$ is not exactly rectangular but approximately so, like the spectrum of $X_N(f)$ (see Appendix B).

When this assumption is made, the Fourier transform of $\tilde{y}_0(t)$ is zero except in rectangular bands of width $2\mu T_0$ centered about $\pm f_0$. Replacing the time-domain convolution in Equation 32 with frequency-domain multiplication and changing variables leads to

$$y_\phi(t) = \frac{1}{\sqrt{\mu}} \left| \int_{-\mu T_0}^{\mu T_0} e^{i\phi(f/\mu T_0)^2} e^{i2\pi ft}\, df \right| . \tag{35}$$

This expression can be evaluated, using formulas 7.4.38 and 7.4.39 from Reference 21, to yield

$$y_\phi(t) = \frac{1}{2} \sqrt{4\mu T_0^2} \sqrt{\frac{\pi}{2\phi}} \left| Z\left[\sqrt{\frac{2}{\pi\phi}} (\pi\mu T_0 t + \phi)\right] - Z\left[\sqrt{\frac{2}{\pi\phi}} (\pi\mu T_0 t - \phi)\right] \right| \tag{36}$$

Evaluating this result at $t = 0$ gives a concise formula for the loss in processing gain:

$$y_\phi(0) = \sqrt{4\mu T_0^2} \sqrt{\frac{\pi}{2\phi}} \left| Z\left(\sqrt{\frac{2\phi}{\pi}}\right) \right| . \tag{37}$$

In the limit for small ϕ, this reduces to the matched case, for

$$\lim_{x \to 0} \frac{Z(x)}{x} = 1 .$$

Equation 37 is plotted in Figure 11 as peak loss in db vs ϕ in radians.

Equation 36, at the time of the Mth expected null, gives the signal amplitude due to slope mismatch as

$$y_\phi\left(\frac{M\delta f}{\mu}\right) = \frac{1}{2} \sqrt{4\mu T_0^2} \sqrt{\frac{\pi}{2\phi}} \left| Z\left[\sqrt{\frac{2}{\pi\phi}} \left(\frac{M\pi}{2} + \phi\right)\right] - Z\left[\sqrt{\frac{2}{\pi\phi}} \left(\frac{M\pi}{2} - \phi\right)\right] \right| . \tag{38}$$

Figures 33 and 36 of Reference 19 suggest that special attention be given to the case $M = \pm 1$, i.e. the leading and lagging anticipated nulls. Figure 12 of this paper plots Equation 38 in normalized form (i.e., for an undistorted peak response of unity).

Equations 37 and 38 and Figures 11 and 12 apply, of course, to all 127 signaling waveforms, not merely the $N = 0$ case. Further, they apply to all rectangular-envelope linear FM pulse-

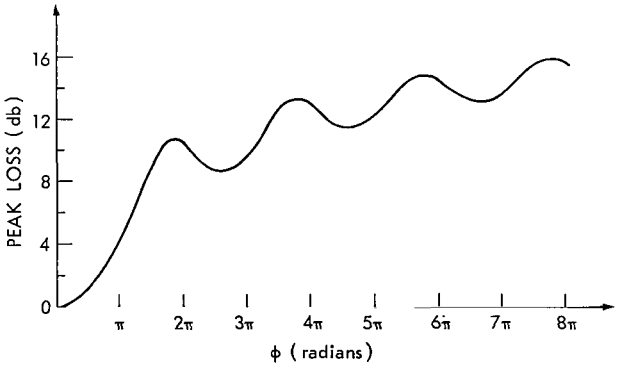

Figure 11—Loss in Γ vs quadratic phase distortion ϕ.

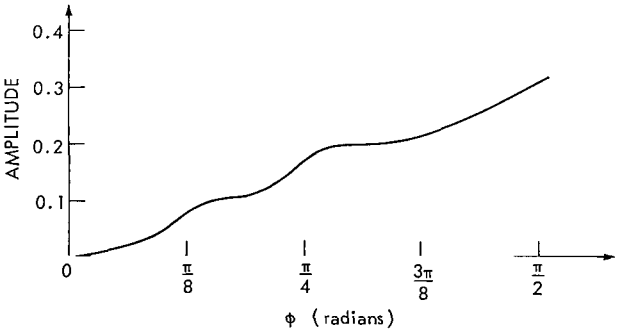

Figure 12—Normalized amplitude of leading and lagging nulls vs ϕ.

compression systems in which the time-bandwidth product Γ is large enough to justify the approximation regarding the residual FM in $\tilde{y}_N(t)$.

Effects of Phase Ripple

Any phase fluctuations of ripples in the transmission system may be considered concentrated in the dispersive delay line proper. The nonlinear group delay associated with the system phase ripple is given by the general formulation

$$t(f) = -\frac{1}{2\pi}\frac{d\phi(f)}{df} . \tag{39}$$

An analytic expression for arbitrary phase ripple in the system passband is given by writing the delay line system function as

$$H_{ph}(f) = A(f)\, e^{i[\phi(f)+\phi_r(f)]} , \tag{40}$$

where, as before,

$$A(f) = 1$$

$$\phi(f) = \frac{\pi}{\mu}(f - f_0)^2$$

and the phase ripple is expressed as a Fourier sine series*

$$\phi_r(f) = \sum_{j=1}^{\infty} a_j \sin j\pi \frac{(f - f_0)}{\Delta f} . \tag{41}$$

The interval of expansion is

$$f_0 - \Delta f \le f \le f_0 + \Delta f ,$$

where

$$\Delta f = 2\mu T_0$$

is the system semi-bandwidth.

*The completness of the representation is not at issue here; the desired phase is neither even nor odd about f_0; small deviations due to tuned circuits, etc., tend to be odd.

The response in the presence of phase ripple is given by the convolution of the undistorted response $\tilde{y}_N(t)$ from Equation 30 with the impulse response of a fictitious filter of system function

$$e^{i\sum_{j=1}^{\infty} a_j \sin j\pi(f-f_0)/\Delta f} .$$

The exponential may be expanded using a well-known Jacobi-Anger formula

$$e^{i\alpha \sin\beta} = \sum_{k=-\infty}^{\infty} J_k(\alpha)\, e^{ik\beta} , \tag{42}$$

where $J_k(\alpha)$ is the Bessel function of the first kind of order k and argument α. If we discard higher-order terms, the impulse response is of the form

$$h_{ph}(t) = J_0(a_1)\,\delta(t) + \sum_{k=1}^{\infty} J_k(a_1)\left[\delta\left(t + \frac{k}{2\Delta f}\right) + (-1)^k\,\delta\left(t - \frac{k}{2\Delta f}\right)\right] , \tag{43}$$

where $\delta(t)$ is the Dirac impulse function. Convolution with $\tilde{y}_N(t)$ produces

$$\tilde{y}_N(t) * h_{ph}(t) = J_0(a_1)\,\tilde{y}_N(t) + \sum_{k=1}^{\infty} J_k(a_1)\left[\tilde{y}_N\left(t + \frac{k}{2\Delta f}\right) + (-1)^k\,\tilde{y}_N\left(t - \frac{k}{2\Delta f}\right)\right] , \tag{44}$$

where the property

$$f(t) * \delta(t - t_0) = f(t - t_0)$$

of the Dirac function has been used freely. The result in Equation 44 is graphically described as "paired echoes"* and suggests (on the basis of energy conservation) the following addition theorem for the squares of Bessel functions:

$$J_0^2(x) + 2\sum_{k=1}^{\infty} J_k^2(x) = 1 .$$

This result was first given by Hansen and is discussed in Section 2.5 of Reference 22.†

Further discussion of the phase ripple problem is best deferred while amplitude ripple is studied.

*A terminology apparently due to Wheeler (Reference 23).
†This may be viewed as a particular consequence of the Parseval theorem. Also, Equation 44 may be considered a time dual of the line spectrum of a carrier angle modulated by a sinusoid.

Effects of Amplitude Ripple

Departures from a flat amplitude characteristic within the system passband can be considered concentrated in the dispersive delay line proper (assuming that their effects are not altered by system nonlinearities such as hard-limiting which may be encountered in satellite repeaters) and writing the system function as

$$H_a(f) = A(f) A_a(f) e^{i\phi(f)} , \tag{45}$$

where $A(f)$ and $\phi(f)$ have been defined above and $A_a(f)$ is expressed as a Fourier cosine* series

$$A_a(f) = \sum_{\ell=0}^{\infty} b_\ell \cos \frac{\ell\pi(f - f_0)}{\Delta f} . \tag{46}$$

The response in the presence of amplitude ripple is then calculated by convolving $\tilde{y}_N(t)$ with the impulse response associated with the system function of Equation 46. Analogous to the phase ripple case, the impulse response is of the form

$$h_a(t) = b_0 \delta(t) + \frac{1}{2} \sum_{\ell=1}^{\infty} b_\ell \left[\delta\left(t + \frac{\ell}{2\Delta f}\right) + \delta\left(t - \frac{\ell}{2\Delta f}\right)\right] . \tag{47}$$

Convolution with $\tilde{y}_N(t)$ again produces paired echoes, but of the form

$$\tilde{y}_N(t) * h_a(t) = b_0 \tilde{y}_N(t) + \frac{1}{2} \sum_{\ell=1}^{\infty} b_\ell \left[\tilde{y}_N\left(t + \frac{\ell}{2\Delta f}\right) + \tilde{y}_N\left(t - \frac{\ell}{2\Delta f}\right)\right] . \tag{48}$$

Combined Effects of Phase and Amplitude Ripple

In view of the basic similarity of the phase-ripple and amplitude-ripple effects, they should be combined into a single mathematical formulation. This is accomplished by multiplication of the system functions $h_{ph}(f)$ and $A_a(f)$ or, equivalently, by convolution of the impulse responses $h_{ph}(t)$ and $h_a(t)$. With the latter, the overall impulse response for superposed amplitude and phase ripples is of the form

$$h_{ph}(t) * h_a(t) = J_0(a_1) b_0 \delta(t) + \sum_{k=1}^{\infty} \left[J_0(a_1) \frac{b_k}{2} + J_k(a_1) b_0\right] \delta\left(t + \frac{k}{2\Delta f}\right) + \sum_{k=1}^{\infty} \left[J_0(a_1) \frac{b_k}{2} + (-1)^k J_k(a_1) b_0\right] \delta\left(t - \frac{k}{2\Delta f}\right) . \tag{49}$$

*Again, the completeness of the representation is not at issue. The desired amplitude characteristic is even about the center frequency, and small departures tend to be even.

If we take only the initial terms (corresponding to the leading and lagging echoes), convolution with $\tilde{y}_N(t)$ yields

$$\tilde{y}_N(t)*h_{ph}(t)*h_a(t) \cong J_0(a_1)\,b_0\,\tilde{y}_N(t)+\left[J_0(a_1)\,\frac{b_1}{2}+J_1(a_1)\,b_0\right]\tilde{y}_N\left(t+\frac{1}{2\Delta f}\right)+\left[J_0(a_1)\,\frac{b_1}{2}-J_1(a_1)\,b_0\right]\tilde{y}_N\left(t-\frac{1}{2\Delta f}\right) \quad (50)$$

Figure 13 illustrates the main response and leading and lagging echoes is given by Equation 50. Higher-order terms which have been discarded in the above formulation correspond to echoes farther removed from the main response, but these in general will be much smaller than the main echoes shown in Figure 13. In the case of arbitrary amplitude and phase ripples, the echo structure will not tend toward symmetry; under certain conditions, e.g.

$$J_0(a_1)\,\frac{b_1}{2} = -J_1(a_1)\,b_0 ,$$

one echo may vanish completely. Further, Equation 50 describes rf signals prior to envelope detection (and not the envelope functions themselves, as indicated in Figure 13 for simplicity). Hence, superposition of leading and lagging echoes on the main response will not necessarily be phase-coherent; an rms superposition of the envelope functions would probably be appropriate.*

Regardless of phase coherence, the loss in Γ due to paired echoes is approximately

$$20\log_{10}\left[J_0(a_1)\,b_0\right] \text{ db} ,$$

which is plotted in Figure 14 for the case $b_0 = 1$.

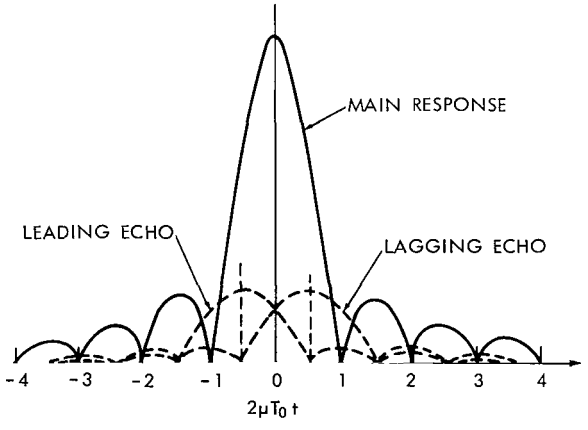

Figure 13—Simplified geometry of paired echoes.

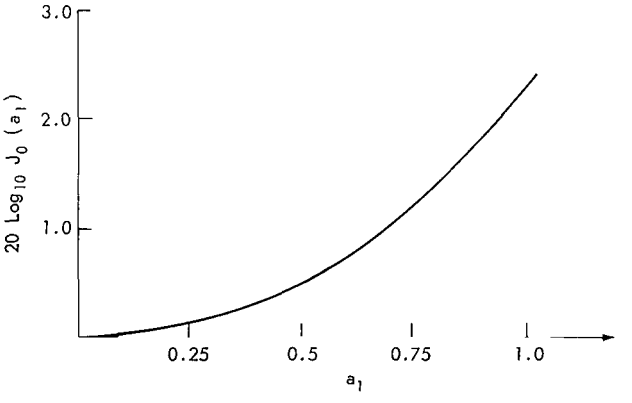

Figure 14—Loss in Γ due to paired echoes.

*Reference 19 contains an exhaustive treatment of the paired-echo superposition problem relative to sidelobe reduction in chirp radar systems. It is noted that the phase coherence of leading and lagging echoes was not taken into consideration in that analysis.

SUMMARY

The theoretical operation of a proposed maximum-likelihood Darlington detector for discretely coded orthogonal PFM signals of unknown phase has been described. It was shown that in principle the communication technique is an ideal M-ary system in the sense defined by Turin.

Anticipated departures from the theoretical system are identified: finite bandwidth in the Fourier transforming dispersive delay line, slope mismatch or quadratic phase distortion, amplitude ripples, and phase ripples. The departure from the ideal characteristic is represented in terms of classical time-invariant linear system theory, and characterized by a system function and/or an impulse response. The analysis derives general results for the effects of the several departures from the ideal (approximating when necessary).

Finite bandwidth produces negligible losses in system-processing gain (because of the large time-bandwidth product of 128) and little significant sidelobe distortion. Slope mismatch leads to serious deteriorations in processing gain and sidelobe waveshape; relatively little quadratic phase distortion can be tolerated in implementing a practical system. Amplitude and phase ripples produce paired echoes that reduce the processing gain and spread out the main response in time, leading to potential intersymbol interference or loss of signaling waveform orthogonality.

The results presented can be used to set upper limits on the departures from the theoretical system, tolerable in implementing the communication technique.

Goddard Space Flight Center
National Aeronautics and Space Administration
Greenbelt, Maryland, July 3, 1967
160-44-05-14-51

REFERENCES

1. King, O. B., "Multiplexing Techniques for Satellite Applications," *Electronics* 32(44), October 1959.

2. "Multiple Access to a Communication Satellite with a Hard-limiting Repeater," Vols. I & II, Report R-108, Institute for Defense Analysis, Washington, D. C., AD 465789.

3. Bedrosian, E., et al., "Multiple Access Techniques for Communications Satellites, I. Survey of the Problem," RM-4298-NASA, September 1964.

4. Schwartz, J., et al., "Modulation Techniques for Multiple Access to a Hard-limiting Repeater," *Proc. IEEE* 54(5), May 1966.

5. Lindholm, C. R., "Multiple Access Techniques for Communication Satellites: Digital Modulation, Time-Division Multiplexing, and Related Signal Processing," The RAND Corporation, RM-4997-NASA, September 1966.

6. Darlington, S., "Demodulation of Wideband, Low-power FM Signals," *Bell Sys. Tech. Jour.* 43(1) Part 2, January 1964.

7. Turin, G. L., "The Asymptotic Behavior of Ideal M-ary Systems," *Proc. IRE* 47(1), January 1959.

8. *Phase A Final Report,* NASA Contract NAS-5-10123, ITT Federal Laboratories, Nutley, N. J.

9. *Phase B Final Report,* NASA Contract NAS-5-10123, ITT Federal Laboratories, Nutley, N. J.

10. Rochelle, R. W., "Pulse-Frequency Modulation Telemetry," NASA TR R-189, Washington, D. C., 1964.

11. Turin, G. L., "Error Probabilities for Binary Symmetric Ideal Reception Through Selective Slow Fading and Noise," *Proc. IRE* 46(9), September 1958.

12. "Transmission Systems for Communications,"Winston-Salem, Bell Telephone Laboratories, 1964, Third edition, Chapter 25.

13. Helstrom, C., "Statistical Theory of Signal Detection," Pergamon Press, 1960, Chapter V.

14. Sos, J., "Signal Detection Techniques for a Discrete-Frequency, Phase Coherent Pulse Frequency Modulation (PFM) Telemetry Signal," *Proc. 1966 Telemetry Conference.*

15. Reiger, S., "Error Rates in Data Transmission," *Proc. IRE* 46(5), May 1958.

16. Golay, M. J. E., "Note on the Theoretical Efficiency of Information Reception with PPM," *Proc. IRE* 37(9), September 1949.

17. Akima, H., "Error rate in a multiple-frequency shift system," *Proc. IEE* 111(3), March 1964.

18. DiFranco, J. and DeLorenzo, J., "Response of a Linear FM Matched Filter to Gated Noise," *Proc. IEEE* 54(6), June 1966.

19. Klauder, J. R., et al., "The Theory and Design of Chirp Radars," *Bell Sys. Tech. Jour.* 39(1), July 1960.

20. DiFranco, J., "Closed Form Solution for the Output of a Finite-Bandwidth Pulse-Compression Filter," *Proc. IRE* 49(6), June 1961.

21. Abramowitz, M. and Stegun, I. A., (editors), "Handbook of Mathematical Functions," National Bureau of Standards AMS 55, Washington, D. C., June 1964.

22. Watson, G. N., "A Treatise on the Theory of Bessel Functions," Cambridge, 1958, second edition.

23. Wheeler, H. A., "The Interpretation of Amplitude and Phase Distortion in Terms of Paired Echoes," *Proc. IRE* 27(6), June 1939.

24. Jahnke, E. and Emde, F., "Tables of Functions," New York: Dover, 1943.

25. Martz, C. W., "Tables of the Complex Fresnel Integral," NASA SP-3010, Washington, D. C., 1964.

Appendix A

The Quadratic Phase Network as a Fourier Transformer; Derivation of Equation 13

This appendix performs three functions. First, it gives a detailed derivation of Equation 13; second, it shows that the pulse-compression phenomenon studied here is only one instance of a much more general Fourier transforming property of quadratic phase networks; and third, it presents all the required computations in step-by-step form, unlike the main text in which few details of the mathematical manipulations were given.

We wish to compute

$$y_N(t) = \left|\tilde{y}_N(t)\right| = \left|x_N(t) * h(t)\right| ,$$

where

$$x_N(t) = \cos 2\pi\left[\left(f_0 + N\delta f\right)t + \frac{\mu t^2}{2}\right] \qquad -T_0 \le t \le T_0$$

$$= 0 \qquad |t| > T_0$$

and

$$h(t) = \int_{-\infty}^{\infty} e^{i2\pi\left[(f-f_0)^2/2\mu - ft_0\right]} e^{i2\pi ft}\, df .$$

We express $x_N(t)$ as the real part of a complex signal $\tilde{x}_N(t)$ and solve for $\tilde{y}_N(t)$ by taking the real part of the complex response. We have

$$\tilde{x}_N(t) = e^{i2\pi\left[(f_0+N\delta f)t+\mu t^2/2\right]} \qquad -T_0 \le t \le T_0$$

$$= 0 \qquad |t| > T_0 .$$

The spectrum of $\tilde{x}_N(t)$ is given by

$$\tilde{X}_N(f) = \int_{-T_0}^{T_0} e^{i2\pi\left[(f_0+N\delta f)\tau+\mu\tau^2/2\right]} e^{-i2\pi f\tau}\, d\tau$$

and

$$\tilde{x}_N(t) * h(t) = \int_{-\infty}^{\infty} \tilde{X}_N(f) H(f) e^{i2\pi f t}\, df$$

$$= \int_{-\infty}^{\infty} \left[\int_{-T_0}^{T_0} e^{i2\pi\left[(f_0+N\delta f-f)\tau+\mu\tau^2/2\right]}\, d\tau \right] e^{i2\pi\left[(f-f_0)^2/2\mu - f(t-t_0)\right]}\, df$$

$$= \int_{-T_0}^{T_0} d\tau \int_{-\infty}^{\infty} e^{i(\pi/\mu)\left[(f-f_0)^2+(\mu\tau)^2+2\mu(f_0+N\delta f)\tau-2\mu f\tau+2\mu f(t-t_0)\right]}\, df \ .$$

Taking $t' = t - t_0$, we rearrange the quantity in brackets to read, after completing the square in the first few terms,

$$\left(f + \mu t' - \mu\tau - f_0\right)^2 + f_0^2 + 2\mu\left(f_0 + N\delta f\right)\tau + (\mu\tau)^2 - \left(\mu t' - \mu\tau - f_0\right)^2 \ .$$

This rearranges after several cancellations to read

$$\left(f + \mu t' - \mu\tau - f_0\right)^2 + (2\mu N\delta f + 2\mu^2 t')\tau - (\mu t')^2 + 2\mu f_0 t' \ .$$

We can now write the complex response as separate f-domain and τ-domain integrals:

$$\tilde{x}_N(t) * h(t) = e^{i2\pi\left[f_0 t' - (\mu t')^2\right]} \int_{-T_0}^{T_0} e^{i2\pi(N\delta f+\mu t')\tau}\, d\tau \int_{-\infty}^{\infty} e^{i(\pi/\mu)\left(f+\mu t'-\mu\tau-f_0\right)^2}\, df \ .$$

The improper f-domain integral can be evaluated by changing variables according to

$$x = \sqrt{\frac{\tau}{\mu}}\left(f + \mu t' - \mu\tau - f_0\right)$$

$$dx = \sqrt{\frac{\pi}{\mu}}\, df$$

to obtain the tabulated integral

$$\int_{-\infty}^{\infty} e^{ix^2}\, dx = \sqrt{\pi i} \ .$$

This yields

$$\tilde{x}_N(t) * h(t) = \sqrt{\mu}\, e^{i2\pi\left[f_0 t - (\mu t'^2/2) + 1/8\right]} \int_{-T_0}^{T_0} e^{i2\pi(N\delta f + \mu t')\tau}\, d\tau \ .$$

Integrating over τ space gives

$$\tilde{x}_N(t) * h(t) = \sqrt{4\mu T_0^2}\, e^{i2\pi\left[f_0 t - (\mu t'^2/2) + 1/8\right]} \frac{\sin 2\pi T_0 (N\delta f + \mu t')}{2\pi T_0 (N\delta f + \mu t')} \ .$$

The real part of the complex response is

$$\tilde{y}_N(t) = \sqrt{4\mu T_0^2} \cos 2\pi \left(f_0 t' - \frac{\mu t'^2}{2} + \frac{1}{8} \right) \frac{\sin 2\pi T_0 (N\delta f + \mu t')}{2\pi T_0 (N\delta f + \mu t')} \ .$$

In regard to the envelope of this expression, disregarding the frequency modulated carrier:

$$y_N(t) = \sqrt{4\mu T_0^2} \left| \frac{\sin 2\pi T_0 (N\delta f + \mu t')}{2\pi T_0 (N\delta f + \mu t')} \right| \ .$$

Finally, $t' = t - t_0$ gives:

$$y_N(t) = \sqrt{4\mu T_0^2} \left| \frac{\sin 2\pi T_0 \left[\mu (t - t_0) + N\delta f \right]}{2\pi T_0 \left[\mu (t - t_0) + N\delta f \right]} \right| \ ,$$

which is Equation 13 of the main text.

The above result is a particular example of a more general phenomenon, namely, the Fourier transforming property of the quadratic phase network. Consider an arbitrary signal of real envelope $\epsilon(t)$ modulated by a complex chirp or linear FM modulation, i.e.

$$x(t) = \epsilon(t) e^{i2\pi\left[f_0 t + (\mu t^2/2)\right]} \ .$$

This chirp modulation may, of course, be superposed on any signal by mixing techniques. Let $X(f)$ be the Fourier transform of $x(t)$, and $E(f)$ be the Fourier transform of $\epsilon(t)$. Now let $x(t)$ drive an all-pass quadratic phase network of system function

$$H(f) = e^{i(\pi/\mu)(f - f_0)^2} \ .$$

The spectrum of the response $y(t)$ is

$$Y(f) = H(f)\,X(f) = \int_{-\infty}^{\infty} H(f)\,x(t)\,e^{-i2\pi ft}\,dt$$

$$= \int_{-\infty}^{\infty} \epsilon(\tau)\,e^{i(\pi/\mu)(f-f_0)^2}\,e^{i2\pi\left[(f_0-f)\tau+(\mu\tau^2/2)\right]}\,d\tau\ .$$

The integrand may be written with a perfect square in the exponent,

$$Y(f) = \int_{-\infty}^{\infty} \epsilon(\tau)\,e^{i(\pi/\mu)\left[(f-f_0)-\mu\tau\right]^2}\,d\tau$$

and the response in the time domain is

$$y(t) = \int_{-\infty}^{\infty}\int_{-\infty}^{\infty} \epsilon(\tau)\,e^{i(\pi/\mu)\left[(f-f_0)-\mu\tau\right]^2}\,e^{i2\pi ft}\,df\,d\tau\ .$$

Equation

$$\left[\sqrt{\frac{\pi}{\mu}}\,(f'-\mu\tau)+\sqrt{\mu\pi}\,t\right]^2 = \frac{\pi}{\mu}\,(f'-\mu\tau)^2 + \mu\pi t^2 + 2\pi f' t - 2\pi\mu t\tau\ ,$$

where

$$f' = f - f_0\ ,$$

gives

$$y(t) = e^{i\left[2\pi f_0 t-\mu\pi t^2\right]}\int_{-\infty}^{\infty} \epsilon(\tau)\,e^{i2\pi\mu t\tau}\int_{-\infty}^{\infty} e^{i\left[\sqrt{\pi/\mu}\,(f'-\mu\tau)+\sqrt{\mu\pi}\,t\right]^2}\,df'\,d\tau\ .$$

Taking

$$\xi = \sqrt{\frac{\pi}{\mu}}\,(f'-\mu\tau) + \sqrt{\mu\pi}\,t\ ,$$

we have

$$\sqrt{\frac{\mu}{\pi}}\int_{-\infty}^{\infty} e^{i\xi^2}\,d\xi = \sqrt{\mu i}$$

and the response is

$$y(t) = \sqrt{\mu i}\, e^{i2\pi\left[f_0 t-(\mu t^2/2)\right]} \int_{-\infty}^{\infty} \epsilon(\tau)\, e^{i2\pi\mu t\tau}\, d\tau \ .$$

The remaining τ space integral is the Fourier transform of $\epsilon(\tau)$ into $-\mu t$ space,

$$y(t) = \sqrt{\mu i}\, E(-\mu t)\, e^{i2\pi\left[f_0 t-(\mu t^2/2)\right]} \ .$$

The above result may be summarized as follows: the quadratic phase network is a Fourier transformer for the envelopes of chirp-modulated signals.

In the system studied in the present essay,

$$\epsilon(t) = \begin{cases} 1 & -T_0 \le t \le T_0 \\ 0 & |t| > T_0 \ , \end{cases}$$

and its Fourier transform is

$$E(f) = \int_{-\infty}^{\infty} \epsilon(t)\, e^{-i2\pi ft}\, dt = \int_{-T_0}^{T_0} e^{-i2\pi ft}\, dt = 2T_0\, \frac{\sin 2\pi f T_0}{2\pi f T_0} \ .$$

Then

$$E(-\mu t) = \sqrt{4T_0^2}\, \frac{\sin 2\pi T_0 \mu t}{2\pi T_0 \mu t}$$

and

$$y(t) = \sqrt{4\mu T_0^2}\, e^{i2\pi\left[f_0 t-(\mu t^2/2)+1/8\right]}\, \frac{\sin 2\pi T_0 \mu t}{2\pi T_0 \mu t} \ .$$

The envelope of the response is

$$\left|y(t)\right| = \sqrt{4\mu T_0^2}\, \left|\frac{\sin 2\pi T_0 \mu t}{2\pi T_0 \mu t}\right| \ ,$$

which is in essence Equation 13 of the main text.

Appendix B

Signal Spectra and System Bandwidth Considerations

The spectra of the actual signaling waveforms $s_N(t)$ are $\sin x/x$ centered at $\pm(f_0 + N\delta f)$ and are unimportant.* This discussion will be concerned with the spectra of the detector waveforms $x_N(t)$. It is these spectra that establish the bandwidth requirements for PFM-to-PPM conversion or spectrum analysis in the dispersive-delay-line demodulator. Formally, the spectrum of any $x_N(t)$ is given by

$$X_N(f) = \int_{-\infty}^{\infty} x_N(t)\, e^{-i2\pi ft}\, dt$$

$$= I_1(f) + I_2(f) ,$$

where

$$I_1(f) = \frac{1}{2}\int_{-T_0}^{T_0} e^{i2\pi\left[(f_0 - f + N\delta f)t + (\mu t^2/2)\right]}\, dt$$

$$= \frac{1}{2}\int_{-T_0}^{T_0} e^{-i2\pi\left[(f_0 + f + N\delta f)t + (\mu t^2/2)\right]}\, dt .$$

In each case, the integration is attacked by completing the square in the exponent along the lines discussed in Appendix A. After the required manipulations,

$$I_1(f) = \frac{e^{-i(\pi\alpha^2/\mu)}}{2\sqrt{2\mu}}\left[Z(b) - Z(a)\right]$$

$$I_2(f) = \frac{e^{-i(\pi\beta^2/\mu)}}{2\sqrt{2\mu}}\left[Z(d) - Z(c)\right] ,$$

*Spectrum truncation due to signal prefiltering is neglected here; as noted in the main text, it is desirable to control the system noise bandwidth by such an operation, and this will reduce the bandwidth requirements of the dispersive delay line accordingly. The present discussion is based on the use of rectangular-envelope chirp signals for simplicity.

where

$$\alpha = \left(f_0 - f + N\delta f\right)$$

$$\beta = \left(f_0 + f + N\delta f\right)$$

$$a = \sqrt{\frac{\Gamma}{2}}\left(\frac{2\alpha}{\Delta f} - 1\right); \qquad c = \sqrt{\frac{\Gamma}{2}}\left(\frac{2\beta}{\Delta f} - 1\right)$$

$$b = \sqrt{\frac{\Gamma}{2}}\left(\frac{2\alpha}{\Delta f} + 1\right); \qquad d = \sqrt{\frac{\Gamma}{2}}\left(\frac{2\beta}{\Delta f} + 1\right) .$$

What can be said of these spectra? First, for positive frequencies, $X_N(f)$ is practically determined by $I_1(f)$ alone. The arguments c and d are so large for all values of f of interest that $I_2(f)$ is vanishingly small as long as system rf and if bandwidths are small compared to rf and if frequencies. This will hold in any practical system. For negative frequencies, $I_2(f)$ effectively defines the spectrum; by symmetry, the signal power spectrum is even about the origin. Hence, system bandwidth requirements can be determined satisfactorily from $I_1(f)$.

Reference 19 shows that the magnitude of $I_1(f)$ is well described by a rectangular function of width $2\mu T_0$ centered at $f_0 + N\delta f$. For large values of the time-bandwidth product Γ, the approximation to a true rectangle is excellent; this is shown in Figures 4, 5, and 6 of Reference 19.

In regard to the several spectra corresponding to all values of N, virtually all the signal power is concentrated in a band of width $4\mu T_0$ centered about f_0. This is the required bandwidth of the dispersive delay line for effective PFM-to-PPM conversion of unprefiltered rectangular envelope system waveforms.

Appendix C

Some Notes on the Complex Fresnel Integral

The complex Fresnel integral has been used extensively in this study of waveform distortion in the Darlington demodulator. This appendix gives definitions, summarizes important properties, and presents several useful results pertaining to the integration of $Z(x)$.

The complex Fresnel integral is defined by

$$Z(x) \equiv \int_0^x e^{i(\pi/2)\xi^2}\, d\xi \ .$$

This holds for all x on the real line and can be extended to complex x as well. $Z(x)$ is a single-valued function that possesses derivatives of all orders everywhere. Figure C1, reproduced from Reference 24, shows $Z(x)$ for small arguments in terms of its real and imaginary parts $C(x)$ and $S(x)$, i.e.

$$Z(x) = C(x) + iS(x)$$

$$C(x) = \int_0^x \cos\left(\frac{\pi}{2}\,\xi^2\right) d\xi$$

$$S(x) = \int_0^x \sin\left(\frac{\pi}{2}\,\xi^2\right) d\xi \ .$$

Also shown in Figure C1 is the fact that if $C(x)$ and $S(x)$ are plotted in rectangular coordinates x, C, and S, they appear as the projections of a spiral in space whose projection on the C, S plane is the famous spiral of Cornu.

Important properties of $Z(x)$ are

$$Z(-x) = -Z(x)$$

$$Z(0) = 0$$

$$Z(\pm\infty) = \pm\left(\frac{1+i}{2}\right) .$$

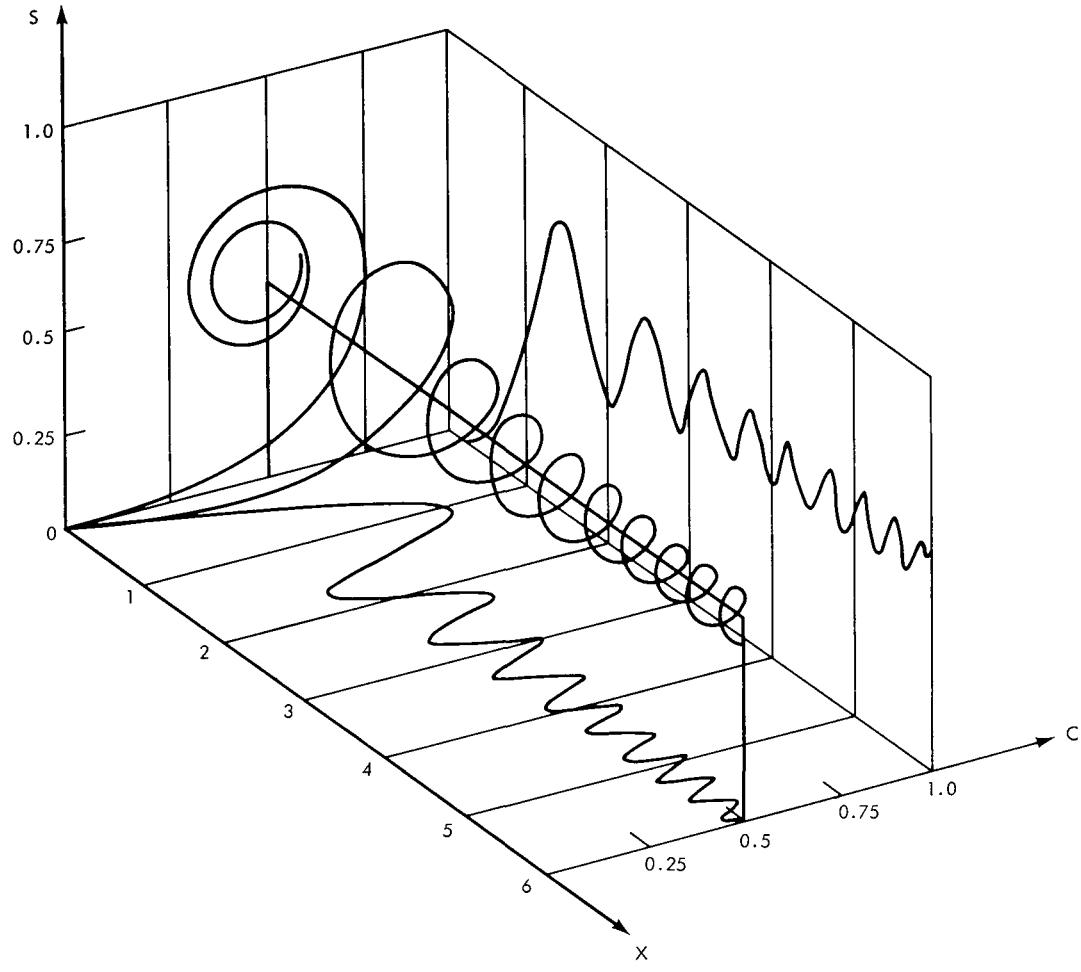

Figure C1—C(X), S(X), and Cornu's spiral.

At several points, this study has used tables of $Z(x)$ in computations and plotting curves. The principal source has been Reference 25; asymptotic forms for large arguments were taken from Reference 21.

Some operations on the Fresnel integral using integration by parts are listed below. The Leibnitz rule for differentiation of the definite integral is also used:

$$\frac{d}{dx}\left[\int_{a(x)}^{b(x)} f(\xi, x)\, d\xi\right] = f\left[b(x), x\right] b'(x) - f\left[a(x), x\right] a'(x) + \int_{a(x)}^{b(x)} \frac{d}{dx}\left[f(\xi, x)\right] dx \ .$$

Result 1—Definite Integral of Z(x)

$$\int_{x_1}^{x_2} Z(x)\, dx = x_2 Z(x_2) - x_1 Z(x_1) + \frac{i}{\pi}\left[e^{i(\pi/2)x_2^2} - e^{i(\pi/2)x_1^2}\right] \ .$$

Result 2—Definite Integral of Z(ax + b)

$$\int_{x_1}^{x_2} Z(ax+b)\,dx = \frac{1}{a}\left[(ax_2+b)\,Z(ax_2+b) - (ax_1+b)\,Z(ax_1+b)\right] + \frac{i}{a\pi}\left[e^{i(\pi/2)(ax_2+b)^2} - e^{i(\pi/2)(ax_1+b)^2}\right]$$

Result 3—Truncated Fourier Transform of Z(x)

$$F(y) = \int_{x_1}^{x_2} Z(x)\,e^{-i2\pi yx}\,dx$$

$$= \frac{i}{2\pi y}\left[e^{-i2\pi yx_2}\,Z(x_2) - e^{-i2\pi yx_1}\,Z(x_1)\right] - \frac{ie^{-2\pi y^2}}{2\pi y}\left[Z(x_2-2y) - Z(x_1-2y)\right] .$$

Result 4—Fourier Transform of a Function Defined by Z(x)

$$f(x) = Z(x+x_0) - Z(x-x_0)$$

$$F(y) = \int_{-\infty}^{\infty} f(x)\,e^{-i2\pi yx}\,dx = 2x_0\sqrt{2i}\;e^{-i2\pi y^2}\,\frac{\sin 2\pi x_0 y}{2\pi x_0 y}$$

Result 3 reduces to Result 2 at the origin, where one must use L'Hospital's rule to evaluate the indeterminate form. Result 4 is of interest, in that it shows that independent of the details of the waveshape of a function defined in terms of Fresnel integrals as written above, its Fourier transform always has a $(\sin x)/x$ envelope. This matter is discussed in connection with passive generation of chirp-radar signals in Reference 19.

"The aeronautical and space activities of the United States shall be conducted so as to contribute . . . to the expansion of human knowledge of phenomena in the atmosphere and space. The Administration shall provide for the widest practicable and appropriate dissemination of information concerning its activities and the results thereof."

—NATIONAL AERONAUTICS AND SPACE ACT OF 1958

NASA SCIENTIFIC AND TECHNICAL PUBLICATIONS

TECHNICAL REPORTS: Scientific and technical information considered important, complete, and a lasting contribution to existing knowledge.

TECHNICAL NOTES: Information less broad in scope but nevertheless of importance as a contribution to existing knowledge.

TECHNICAL MEMORANDUMS: Information receiving limited distribution because of preliminary data, security classification, or other reasons.

CONTRACTOR REPORTS: Scientific and technical information generated under a NASA contract or grant and considered an important contribution to existing knowledge.

TECHNICAL TRANSLATIONS: Information published in a foreign language considered to merit NASA distribution in English.

SPECIAL PUBLICATIONS: Information derived from or of value to NASA activities. Publications include conference proceedings, monographs, data compilations, handbooks, sourcebooks, and special bibliographies.

TECHNOLOGY UTILIZATION PUBLICATIONS: Information on technology used by NASA that may be of particular interest in commercial and other non-aerospace applications. Publications include Tech Briefs, Technology Utilization Reports and Notes, and Technology Surveys.

Details on the availability of these publications may be obtained from:

SCIENTIFIC AND TECHNICAL INFORMATION DIVISION

NATIONAL AERONAUTICS AND SPACE ADMINISTRATION

Washington, D.C. 20546